Reconstructing the Topology of Optical Polarization Knots

Hugo Larocque[1], Danica Sugic[2], Dominic Mortimer[1], Alexander J. Taylor[2], Robert Fickler[1], Robert W. Boyd[1,3], Mark R. Dennis[2,4], and Ebrahim Karimi[1,5,*]

[1]Department of Physics, University of Ottawa, Ottawa, Ontario, K1N 6N5, Canada

[2]H. H. Wills Physics Laboratory, University of Bristol, Bristol BS8 1TL, UK

[3]Institute of Optics, University of Rochester, Rochester, New York, 14627, USA

[4]School of Physics and Astronomy, University of Birmingham, Birmingham, B12 2TT, UK

[5]Department of Physics, Institute for Advanced Studies in Basic Sciences, 45137-66731 Zanjan, Iran

Knots are topological structures describing how a looped thread can be arranged in space. Though most familiar as knotted material filaments, it is also possible to create knots in singular structures within three-dimensional physical fields such as fluid vortices[1] and the nulls of optical fields[2-4]. Here we produce, in the transverse polarization profile of optical beams, knotted lines of circular transverse polarization. We generate and observe both simple torus knots and links as well as the topologically more complicated figure-eight knot. The presence of these knotted polarization singularities endows a nontrivial topological structure on the entire three-dimensional propagating wavefield. In particular, the contours of constant polarization azimuth form Seifert surfaces of high genus[5], which we are able to resolve experimentally in a process we call *seifertometry*. This analysis reveals a level of topological complexity, present in all experimentally generated polarization fields, that goes beyond the conventional reconstruction of polarization singularity lines.

Many physical systems enclose regions that have a singular nature, often manifested as curves in three-dimensional space carrying a discrete physical quantity. For instance, in superconductors, the singularities of the magnetic field carry quantized units of magnetic flux[6], while in superfluids, the singularities of the wavefunction carry quantized circulation[7]. Similar structures also occur within optical beams, where they manifest as singular lines of optical phase along zeros of the amplitude, known as wave dislocations or optical vortices[8-10]. These strands form complex self-winding looped three-dimensional structures that can even adopt knotted configurations. Although not so obvious as the knotted singularities themselves, such configurations also affect the topology of other structures in the surrounding wavefield. Namely, the singularities bound a space-filling structure of twisted phase sheets, i.e. surfaces where the phase of the wavefield is constant, whose physical properties may be analyzed as topological objects in their own right.

Knotted phase singularities have been both theoretically and experimentally demonstrated in optical beams[2-4]. However, only torus knots, which can be represented as multi-strand helices wrapped around a torus, have previously been successfully generated experimentally in optical fields[3-4]. The simplicity of the torus knot prescription, especially the trefoil knot, has led these to be chosen as examples of knots generated in physical systems such as fluid vortices[1] and

colloidal particles configuring liquid crystals[11]. Other knots can have a more involved structure, requiring twisting and crossing in multiple directions, which can be constructed theoretically in complex scalar fields[12,13], but are more technically challenging to implement experimentally. For any optical vortex knot, the full characterization of the phase structure of the surrounding amplitude is generally a difficult task given that the knots reside in low-intensity regions of the beam which are bright elsewhere. A full reconstruction of the topology of the field around the knot reveals extra topological information about how the phase surfaces are globally inter-nested[12]. Being oriented, these are *Seifert surfaces* for the knot[5], and the set of all Seifert surfaces fills the three-dimensional space occupied by the field's intensity. However, these surfaces break down at three-dimensional critical points of the phase that are analogous to certain types of phase saddles[14]. These points are locally diabolos across which the integer genus of the Seifert surfaces (i.e. the number of bridges/holes on the surface) jumps by ±1. The total absence of these critical points would give a fibered knot[5,13], and is mathematically possible for torus knots and other structures such as the figure-eight knot[13]. Other knots however are defined by a Morse-Novikov index indicating the minimum number of critical points[12]. Here we demonstrate a method of analyzing the Seifert surface structure–seifertometry–of the polarisation ellipse orientations around various knotted polarisation singularities.

Polarization singularities are associated with an optical field's electric field vector, which, in a beam propagating along the z-direction, in general executes an ellipse in the xy-plane[9,10,15-17]. Both the ellipse shape (i.e. ellipticity), and orientation (i.e. polarization azimuth), are determined by Stokes parameters, s_1, s_2, s_3, and vary with x,y,z. The ellipse is circular at points in two dimensions, known as *C-points*, and along lines in three dimensions, known as *C-lines*[9,10], where the polarization azimuth is undefined. Such polarization singularities organize the topological structure of the ellipse fields in the same way that vortex lines organize the optical phase. When longitudinal polarization is also included, C-lines acquire more complicated three-dimensional properties manifested as optical Möbius bands[18-22].

Beams carrying polarization singularities can be generated by means of a coherent superposition of structured left- and right-handed circularly polarized light[16,17]. In particular, the relative spatial intensity profiles of both polarizations define the ellipticity profile of the resulting beam. Likewise, the relative spatial phase profiles of both circular components determine the polarization ellipse azimuth. Therefore, beams that carry C-lines can readily be produced by superposing a circularly polarized beam carrying phase singularities with an oppositely polarized beam that has a smooth phase profile.

The core of our method to generate optical polarization knots relies on the above superposition principles and the use of holographic beam shaping methods that allow precise control over a beam's intensity and phase profile[23]. Further details regarding the employed generation scheme can be found in Fig. 1, the Methods, and the Supplementary Information. Namely, this scheme creates a space-varying polarized light beam with C-line singularities that undergo knotted trajectories upon free-space propagation. For such beams, the wavefield in which the knot is encoded consists of the complex Stokes field $s_1 + i\, s_2$, whose phase corresponds to twice the value of the polarization azimuth. The dynamics of the knotted C-lines are examined by measuring the optical field's Stokes parameters from which a complete reconstruction of the beam's polarization pattern can be performed. These measurements also allow us to resolve sheets of constant polarization azimuth that terminate on the knot itself.

With this method, we reconstruct the contour surfaces on which the ellipse azimuth is constant and that form our polarization knots' Seifert surfaces. In Fig. 2a,b we show the experimental and theoretical trefoil knot, one of its Seifert surfaces, and cross-sectional images of the knot's polarization ellipse profile. We also perform similar experimental reconstructions of torus knots and a choice of azimuth Seifert surface for the Hopf link in Fig. 2c and cinquefoil knot in Fig. 2d, the other knot and link structures which were previously experimentally generated[4]. The knot types are sufficiently simple to be classified by visual inspection, emphasized by appropriate projections in the figure, but we have also confirmed them by standard mathematical knot identification procedures summarized in the Methods[24]. The chosen Seifert surface for the knots in Fig. 2 seem to be the simplest surfaces spanning the knot; in the Supplementary Information, we observe that these particular surfaces have minimal genus.

In Fig. 3, we show the results of the first experimental generation of a figure-eight knot engineered in an optical field. This kind of knot must be embedded in a field of sufficient complexity stated to be beyond the capability of previous implementations[4]. Using an improved hologram design[13], our polarimetric measurements were sensitive enough to resolve and characterize its complex three-dimensional pattern, which appears to have distinctly more structure than the torus knots discussed previously. The knot obtained from our experiments can be found in Fig. 3a next to its expected structure shown in Fig. 3b. Seifert surfaces for different polarization azimuths are shown in Fig. 3c,d. The topology of these surfaces, quantified by their genus, is different between theory and experiment. In Fig. 3e, we plot, as a function of azimuth, the experimental and theoretical genus of the closed surface join of Seifert surfaces for orthogonal polarization azimuths. The numerical procedure for calculating the genus is described in the Methods: the choice to use closed surfaces avoids numerical sampling issues at the knotted boundary of the polarization surfaces, but does not otherwise affect the analysis. We call the analysis of the continuous set of surfaces, and their quantification via genus, the seifertometry of the knotted complex polarization field (the same analysis is performed for torus knots in the Supplementary Information).

Theoretically, for almost all values of azimuth except those close to 0 and $\pi/2$, the genus takes the minimal value of 1 for each of the Seifert surfaces, and 2 in small intervals around 0 and $\pi/2$, which are doubled when the surfaces are joined. An illustration of the genus discontinuities close to 0 is shown in Fig. 3 f; as the azimuth increases through 0, two bridges on the Seifert surfaces appear then break through diabolos situated at 3D critical points (in fact corresponding to the 2D cyan saddle points in Fig. 3b). Experimentally however, values of genus from 2 up to about 16 are found in the measured volume, despite the knotted singularity being preserved. This indicates that the topology of the experimental Seifert surfaces is strongly disrupted by the presence of extra critical points in the azimuth function, each of which causes the genus to jump. The maximum genus occurs where the azimuth is near to 0 and $\pi/2$, as with the theoretical plot, indicating these surfaces are particularly unstable and 3D critical points may tend to occur close to these values. This is due to experimental imperfections such as aberrations, which are sufficiently small to ensure the existence of the rather complicated figure-eight knot structure in the polarization singularity lines, but cause the existence of critical points in the azimuth elsewhere in the 3D volume. Achieving agreement of the genus of constant azimuth surfaces with the theoretical profile seems to be much more challenging than simply realizing knotted singular lines.

Such seifertometric measurements could help illuminate the difficulties in forming particular types of knotted fields, and for instance could be used to optimize beam parameters by stabilizing their polarization structures rather than by adjusting the shape of the singularities themselves. Smoothing experimental imperfections will cause the critical points to move and react with each other, eventually causing them to annihilate to a minimal number. However, our results indicate that these events are far more subtle and delicate even than manipulating polarization singularity lines, and their topological processes are currently not understood in optical fields.

To summarise, we demonstrated the ability to generate optical polarisation fields with mathematically nontrivial 3D topology, by creating knotted polarisation singularities in the form of torus knots and links, and the figure-eight knot, and showing that they can be accurately characterized by means of polarimetric measurements. This allows detailed reconstruction of a knotted field's structural elements, especially its Seifert surfaces, and we described the basis of our seifertometric analysis. Our method could lead to the development of schemes used to generate and characterize more complicated optical structures[12,13] that are of fundamental or applied interest. Though our intricate apparatus allows for the generation of highly customizable structures, it could also potentially be scaled down using devices that are routinely used to produce polarization singularities[17,25]. Such devices could be used to generate simpler structures with less aberrations that could be practical for applications. The quantum nature of these knots[26] could also be explored within the framework of polarization pattern entanglement[27,28]. The idea of seifertometry can also be extended to random polarization fields, whose three-dimensional singular lines were studied in[14], and in which a wide variety of knots have been found in large-scale simulations[29]. Finally, the generation of our polarization structures motivates their study in physical systems that display exotic nonlinear dynamics when illuminated with space-varying polarized light beams[30]. For instance, the seifertometry procedure could be used to investigate nonlinearly induced critical points in the knot's structure.

References:

1. Kleckner, D. & Irvine, W. T. M. Creation and dynamics of knotted vortices. *Nat. Phys.* **9**, 253-258 (2013).
2. Berry, M. V. & Dennis, M. R. Knotted and linked phase singularities in monochromatic waves. *Proc. R. Soc. A* **457**, 2251-2263 (2001).
3. Leach, J., Dennis, M. R., Courtial, J. & Padgett, M. J. Laser beams: knotted threads of darkness. *Nature* **432**, 165 (2004).
4. Dennis, M. R., King, R.P., Jack, B., O'Holleran, K. & Padgett, M. J. Isolated optical vortex knots. *Nat. Phys.* **6**, 118-121 (2010).
5. Adams, C. C. *The Knot Book: An Elementary Introduction to the Mathematical Theory of Knots* (American Mathematical Society, 2004).
6. Abrikosov, A.A. On the magnetic properties of superconductors of the second group. *Sov. Phys. JETP* **5,** 1174 (1957).
7. Donnelly, R. J. *Experimental Superfluidity* (University of Chicago Press, 1967).
8. Nye, J. F. & Berry, M. V. Dislocations in wave trains. *Proc. Roy. Soc. A.* **336**,165-190 (1974).

9. Nye, J. F. *Natural Focusing and Fine Structure of Light* (IoP Publishing, 1999).
10. Dennis, M. R., O'Holleran, K. & Padgett M. J. Singular optics: optical vortices and polarization singularities. *Prog. Opt.* **53**, 293-363 (2009).
11. Martinez, A., Ravnik, M., Lucero, B., Visvanathan, R., Žumer, S. & Smalyukh, I. I. Mutually tangled colloidal knots and induced defect loops in nematic fields. *Nat. Mater.* **13**, 258-263 (2014).
12. Dennis, M. R. & Bode, B. Constructing a polynomial whose nodal set is the three-twist knot 52. *Journal of Physics A: Mathematical and Theoretical* **50**, 265204 (2017).
13. Bode, B., Dennis, M. R., Foster, D. & King, R. P. Knotted fields and explicit fibrations for lemniscate knots. *Proc. R. Soc. A* **473**, 20160829 (2017).
14. Nye, J. F. Phase saddles in light beams. *J. Opt.* **13**, 075709 (2011).
15. Flossmann, F., O'Holleran, K., Dennis, M. R., Padgett, M. J. Polarization singularities in 2D and 3D speckle fields. *Phys. Rev. Lett.* **100**, 203902 (2008).
16. Galvez, E. J., Khadka, S., Schubert, W. H. & Nomoto, S. Poincaré-beam patterns produced by nonseparable superpositions of Laguerre–Gauss and polarization modes of light. *Appl. Opt.* **51**, 2925-2934 (2012).
17. Cardano, F., Karimi, E., Marrucci, L., de Lisio, C. & Santamato, E. Generation and dynamics of optical beams with polarization singularities. *Opt. Express* **21**, 8815-8820 (2013).
18. Freund, I. Optical Möbius strips in three−dimensional ellipse fields, *Opt. Commun.* **283**, 1−15 (2010).
19. Bauer, T., Banzer, P., Karimi, E., Orlov, S., Rubano, A., Marrucci, L., Santamato, E., Boyd, R. W. & Leuchs, G. Observation of optical polarization Möbius strips. *Science* **347**, 964-966 (2015).
20. Bauer, T., Neugebauer, M., Leuchs, G. & Banzer, P. Optical polarization Möbius strips and points of purely transverse spin density. *Phys. Rev. Lett.* **117**, 013601 (2016).
21. Galvez, E. J., Dutta, I., Beach, K., Zeosky, J. J., Jones, J. A., & Khajavi, B. Multitwist Möbius strips and twisted ribbons in the polarization of paraxial light beams, *Scientific Reports* **7**, 13653−13656 (2017).
22. Garcia-Etxarri, A., Optical polarization Möbius strips on all−dielectric optical scatterers, *ACS Photonics* **4**, 1159−1164 (2017).
23. Bolduc, E., Bent, N., Santamato, E., Karimi, E. & Boyd, R. W. Exact solution to simultaneous intensity and phase encryption with a single phase-only hologram. *Opt. Lett.* **38**, 3546 (2013).
24. Taylor, A. J. & other SPOCK contributors. pyknotid knot identification toolkit v0.5.3. https://github.com/SPOCKnots/pyknotid, Accessed 2018-05-09 (2018).
25. Larocque, H., Gagnon-Bischoff, J., Bouchard, F., Fickler, R., Upham, J., Boyd, R. W. & Karimi, E. Arbitrary optical wavefront shaping via spin-to-orbit coupling. *J. Opt.* **18**, 124002 (2016).
26. Romero, J., Leach, J., Jack, B., Dennis, M. R., Franke-Arnold, S., Barnett, S. M. & Padgett, M. J. Entangled optical vortex links. *Phys. Rev. Lett.* **106**, 100407 (2011).
27. Fickler, R., Lapkiewicz, R., Ramelow, S. & Zeilinger, A. Quantum entanglement of complex photon polarization patterns in vector beams. *Phys. Rev. A* **89**, 060301 (2013).
28. Karimi, E., Leach. J., Slussarenko, S., Piccirillo, B., Marrucci, L., Chen, L., She, W., Franke-Arnold, S., Padgett, M. J. & Santamato, E. Spin-orbit hybrid entanglement of photons and quantum contextuality. *Phys. Rev. A* **82**, 022115 (2010).

29. Taylor, A. J. & Dennis, M. R., Vortex knots in tangled quantum eigenfunctions. *Nat. Commun.* **7**, 12346 (2016).
30. Bouchard, F., Larocque, H., Yao, A. M., Travis, C., De Leon, I., Rubano, A., Karimi, E., Oppo, G.-L. & Boyd, R. W. Polarization shaping for control of nonlinear propagation. *Phys. Rev. Lett.* **117**, 233903 (2016).

Acknowledgments: The authors thank Frédéric Bouchard for his advice on using the SLM and Peter Banzer for fruitful discussions. This work was supported by Canada Research Chair (CRC) and Canada Foundation for Innovation (CFI). R.F. acknowledges the financial support of the Banting postdoctoral fellowship of the NSERC. E.K. and R.W.B. acknowledge the support of the Canada Excellence Research Chairs (CERC) Program. D.S, A.J.T and M.R.D were supported by the Leverhulme Trust Research Programme Grant No. RP2013-K-009, SPOCK: Scientific Properties of Complex Knots.

Author Information: Correspondence and requests for materials should be addressed to ekarimi@uottawa.ca.

Competing interests: The authors declare no competing interests.

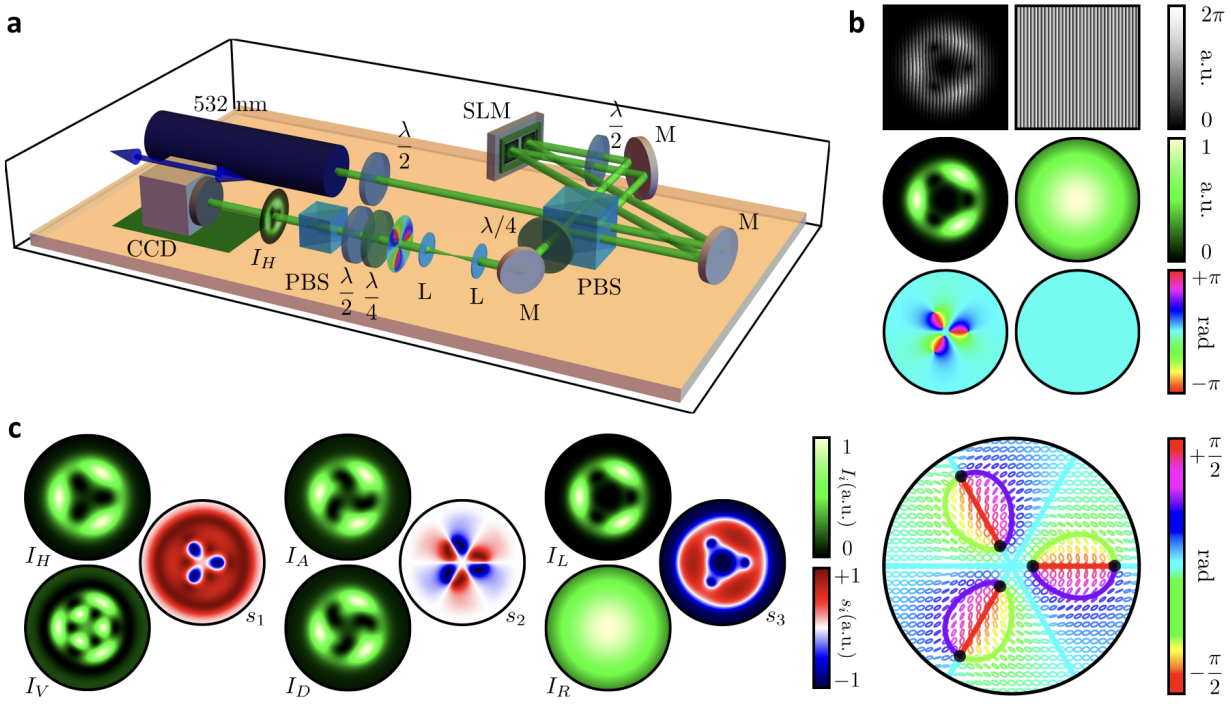

Fig. 1. **Schematic of the experimental apparatus used to generate and characterize polarization singularity knots. a,** Linearly polarized light emitted from a 532 nm diode laser is sent through a half-wave plate (HWP) balancing the beam's horizontal and vertical polarization components. These components are then separated by a polarizing beam splitter (PBS) and sent through a folded Sagnac interferometer where each polarization component is individually modulated by a spatial light modulator (SLM) into a beam carrying knotted phase singularities

and a Gaussian beam, respectively. The two beams, that now have different transverse modulations in addition to being orthogonally polarized, then exit the interferometer where they become superimposed. A quarter-wave plate (QWP) alters the two modulated linearly polarized components into circularly polarized beams, thus producing a space-varying polarized light beam carrying knotted C-lines. The beam is then imaged using two lenses (L) in order to probe the knotted dynamics of the C-lines. The beam's characterization is performed through polarization tomography relying on a sequence of a QWP, a HWP, a PBS, and a CCD camera. **b,** The SLM configuration used to produce beams carrying polarization singularity knots. Two holograms designed to individually modulate each component in the interferometer are placed side by side on the SLM as shown above. The intensity and phase profiles of the resulting beams are shown below the holograms, respectively. The images on the left correspond to the component with knotted phase singularities forming a trefoil knot upon propagation while the other consists of the Gaussian component with a flat phase front. **c,** Required tomographic measurements attributed to the components shown in **b**. Namely, the intensity of horizontal (I_H), vertical (I_V), anti-diagonal (I_A), diagonal (I_D), left (I_L), and right (I_R) polarized components are used to calculate the beam's reduced Stokes parameters s_1, s_2, and s_3, which are thereafter employed to reconstruct the polarization profile of the beam and extract its polarization orientation profile. This profile is shown on the far right and highlights the regions carrying C-points along with four contours of constant azimuth that are coloured based on the value to which they are associated. Figure legends: λ/2: half-wave plate, λ/4: quarter-wave plate, M: mirror, and L: lens.

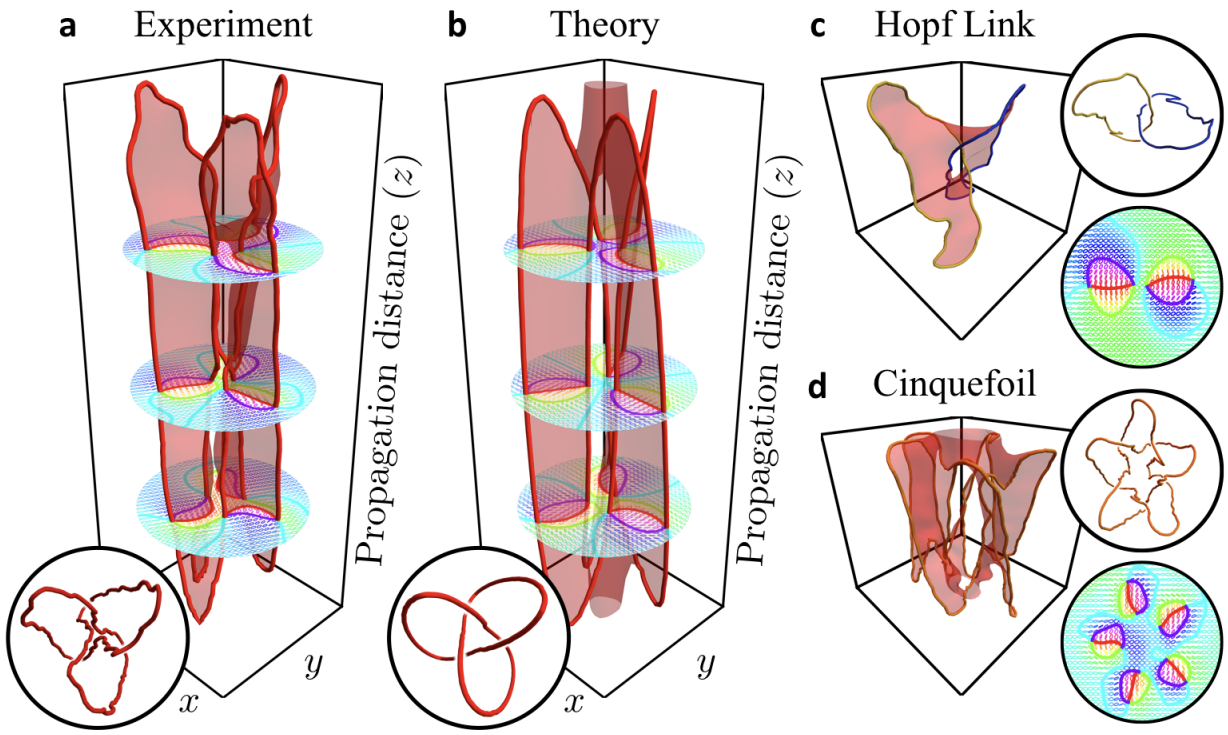

Fig. 2. **Topological traits of torus structures.** Depiction of the various entities attributed to an optical trefoil knot corresponding to **a,** experimental and **b,** theoretical results. In this display, the knotted trajectories of the C-lines are shown in red and the Seifert surface defined by regions

with an azimuth of ±π/2 are displayed in red. The transverse polarization profile of the optical knot is shown for different propagation distances as cross-sectional images. A similar experimental surface reconstruction is performed for other torus structures including **c,** a Hopf link, and **d,** a cinquefoil knot. The polarization profile in the focal plane of these optical structures is shown at the bottom right corner of the surfaces. All three dimensional images are accompanied by a top view image in which crossings have been made more noticeable. The aspect ratios of the plots were chosen to better depict the main features of the knots' structure and do not necessarily scale to the real dimensions of the knots. Additional details surrounding the knots' dimensions can be found in the Methods.

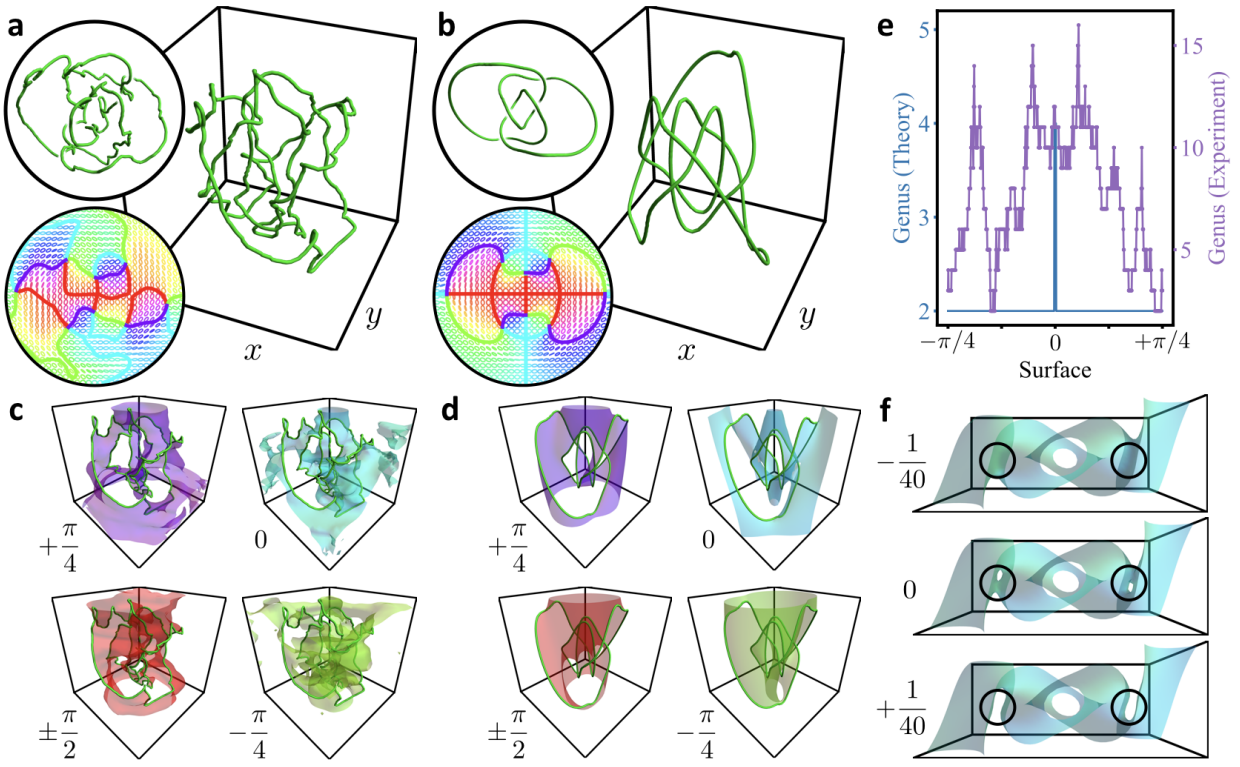

Fig. 3. **Topological characterization and seifertometry of an optical figure-eight knot** Optical polarization figure-eight knots reconstructed from **a,** experiment and **b,** theory along with the knotted beam's polarization structure at the focal plane and an axial view in which crossings have been emphasised. The Seifert surfaces of these structures are shown in **c,** and **d,** respectively, where they are labeled by the polarization azimuth value attributed to the surface. Enlarged versions of these surfaces can be found in the Supplementary Information. **e,** Numerically extracted genus of the closed surfaces which are the join of pairs of Seifert surfaces with azimuth values different by π/2 (see Methods). In theory, the genus remains constant except in the vicinity of the 0 orientation surfaces where it spikes due to the addition of two holes in the surface as shown in **f,** where surfaces with an azimuth of -1/40, 0 and +1/40 are shown.

Methods

Generation scheme for optical polarization knots. As shown in Fig. 1, by means of a folded Sagnac interferometer[26,31], we can produce a beam defined by distinct opposite circular polarizations, one of which is defined by phase vortices that experience knotted trajectories upon propagation, and the other consisting of a conventional Gaussian beam that is sufficiently large to match the transverse extent of the knotted component. Each of these two beams are modulated by means of phase holograms that simultaneously structure their intensity and phase profiles[23] in order to precisely produce optical configurations displaying knotted dynamics. The beam resulting from this superposition therefore consists of a space-varying polarized light beam with C-line singularities that undergo knotted trajectories upon free-space propagation. By measuring the beam's Stokes parameters, we can perform a polarimetric reconstruction of its transverse polarization distribution. This distribution thereafter allows us to resolve the positions of the C-lines and of sheets of constant polarization azimuth that terminate on the knot itself. To generate our knots, we specifically employ computer generated holograms that are displayed on a spatial light modulator (Holoeye, Pluto series). Specific details regarding the holograms themselves are provided in the Supplementary Information. In consideration of the imaging lenses in the setup, which reduced the knots' beam size by a factor of ⅖, these holograms produced optical knots defined by a transverse extent of roughly 1 mm and a length varying between 15 to 30 cm depending on the generated knot. Polarization measurements are recorded by means of a CCD camera (Thorlabs DCU223C).

Characterization limitations of optical knots with phase singularities. From a practical point of view, measuring knotted polarization singularities by polarimetry is a more accurate way of characterizing the structure of knotted optical fields than measuring optical vortices in scalar fields by either intensity measurements or phase contrast. Superposing an orthogonally polarized component without vortices to a scalar field containing a knotted vortex reduces the variation of overall intensity across the light beam, whereas optical vortices occur in low-intensity regions[32]. For scalar field measurements[4], the only way phase can be determined is by interfering the hologram's phase with a sequence of reference waves. Since the detector contrast is optimized for dark regions, measurements become oversaturated in higher-intensity regions. Here, the polarization azimuth around the knotted polarization singularities, analogous to the scalar phase, is determined directly from measured Stokes parameters.

Procedures for numerical seifertometry. The numerical procedure for calculating the genus of the polarization surfaces is as follows, and uses certain standard methods for the topological analysis of surfaces. First, rather than taking every surface separately, it is numerically simpler to trace the pair of surfaces with azimuths φ, $\varphi+\pi/2$, which together form a smooth surface passing through the knotted singularity. The genus of the surfaces is additive, so this does not affect the

quality of the results but avoids introducing unnecessary boundaries. The input to the genus calculation is then an array of complex numbers representing the value of the wavefield at different points, which may be obtained numerically or experimentally. The surfaces of constant argument of the complex numbers, corresponding to surfaces of constant polarization azimuth, are extracted using the standard "marching cubes" algorithm which returns a numerical triangulation of the surface[33].

This triangulation can then be used to obtain the surface's Euler characteristic $\chi = V - E + F$, where V is the number of distinct triangle vertices, E is the number of distinct edges, and F is the number of triangle faces. Note that most vertices and edges are shared between triangles, except on boundaries of the surface. Finally, the genus is obtained as $g = (b - \chi + 2)/2$, where b is the number of boundary components of the triangulation. This numerical procedure is simple but efficient, and it is easily practical to sample many tens or hundreds of different polarization surfaces from a given input array.

The main limitations of this procedure come from the resolution of the input measurements, as the recovered surfaces essentially arise from linear interpolation between the measured points of the field. This does not appear to be a major issue, as the experimental resolution is high on the scale of the knotted structures, and the polarization sheets are recovered without difficulty. It is also important that the genus is a topological quantity, and so is not affected by distortions in the approximated local geometry.

Identifying Knots. In general our curves are sufficiently simple that their knot type can be determined by visual inspection, made easier by appropriate choices of projection as shown in Fig. 2 and Fig. 3a-b. However, this is unsatisfactory as a method for automated data analysis, and we have also confirmed the knotting by mathematical calculation.

The knot type is found algorithmically by calculating "knot invariants" of the curve. These are functions that depend only on its knot type, regardless of the local geometry[5]. The knot is found by calculating one or more invariants, then finding the knot type from a pre-determined knot catalogue. Knot invariants are not in general perfect discriminators of different knots, but when the curves are not very tangled (as in our data) even simple choices are sufficient to unambiguously determine their topology.

We detect our knot types using primarily the standard Alexander polynomial invariant, implemented in the pyknotid knot identification toolkit[24] (the algorithm is standard[34]). The Alexander polynomial is easy to calculate but not an especially discriminatory choice compared to more powerful invariants. However, our knotted vortices are geometrically relatively simple, even if this is not clear to the eye. This allows the numerical routines to bound the maximum possible complexity of its knot topology, identifying the curve unambiguously as the single specific knot we expect.

References:

31. Fickler, R. Lapkiewicz, R., Plick, W. N., Krenn, M., Schae, C., Ramelow, S. & Zeilinger, A. Quantum entanglement of high angular momenta. *Science* **338**, 640-643 (2012).

32. Padgett, M. J., O'Holleran, K., King, R. P. & Dennis, M. R. Knotted and tangled threads of darkness in light beams. *Contemporary Physics* **52**, 265-279 (2011).

33. Lorensen, W. E. & Cline, H. E. Marching cubes: a high resolution 3d surface construction algorithm. *ACM Computer Graphics* **21**, 163-169 (1987).

34. Orlandini, E. & Whittington, S. G. Statistical topology of closed curves: some applications in polymer physics. *Rev. Mod. Phys.* **79**, 611-642 (2007).